TAF Journal of Advances in Technology and Engineering Studies JATER
2017, **3**(5): 192-210

PRIMARY RESEARCH

The failure of delayed detached eddy simulation for flow control over a hump using synthetic jet actuator

Mohamed A. Mohamed [1*], **Qin Ning** [2]

[1] School of Engineering, University of South Wales, Pontypridd, UK

[1] Department of Mechanical Engineering, Faculty of Engineering, South Valley University, Qena, Egypt

[2] Department of Mechanical Engineering, University of Sheffield, Sheffield, UK

Index Terms
URANS
DES
DDES
Steady Suction Control
Synthetic
Jet Control

Received: 21 July 2017
Accepted: 7 August 2017
Published: 9 October 2017

***Abstract*—** The performance of three different numerical methods for predicting the large separated flow over a hump model and its control using steady suction and techniques is investigated. Unsteady Reynolds Averaged Navier-Stokes (URANS), Detached Eddy Simulation (DES) and Delayed Detached Eddy Simulation (DDES) approaches are developed and applied to determine the proficiency of these approaches in predicting such degree of separation and assess their applicability to capture the turbulent flow structures in the separated flowfield. Active flow control techniques are applied by means of two-dimensional slot located at x/c≈0.65 along the model spanwise with an opening of 0.00187c, directly upstream on the concave surface. The novelty of the present work is that the dynamic grid technique is formulated to model the repeated motion of the synthetic jet membrane instead of using the oscillating boundary conditions at the jet exit. Dynamic grid is found to be useful in providing more insight into the physical mechanism that drive the interface between the plenum flow and separated boundary layer flow. The numerical results obtained from the baseline and controlled cases are validated against the measurements and compared with published numerical results in terms of mean flow quantities. Despite the fact that URANS and DES methods provide good agreement with the measurements for the uncontrolled and steady suction controlled cases, only DES showed the flow unsteadiness, however the DDES method failed to predict the mean flow quantities or the turbulent flow features. The dynamic grid technique successfully simulated the cavity flow, showed up the existence of two counter rotating vortices inside the plenum move up and down during the control cycle and finally energized the boundary layer in the separated flow region.

I. INTRODUCTION

Flow separation control using active methods such as steady suction/blowing and synthetic jets with Zero Net Mass Flux was studied extensively by many researchers. Numerous experimental [1, 2, 3, 4, 5, 6, 7, 8, 9, 10, 11, 12] and numerical [13, 14, 15, 16, 17] studies were conducted in this area. Numerical methods using Computational Fluid Dynamics (CFD) techniques were widely used for simulating and evaluating the synthetic jets as active flow method in controlling the flow separation over lifting surfaces. To investigate the capabilities of different numerical methods in predicting the synthetic jet flow and separation control, NASA Langley Research Centre carried out a CFD workshop [18] for this purpose [18]. In that workshop, three different cases were studied in which the flowfield is generated through a rectangular slot in a quiescent environment [19], a circular oscillatory jet issuing into a crossflow over a flat plate [20] and through a rectangular slot over a wall-mounted hump [21, 22, 23]. Flow unsteadiness, motion of vortex pairs and transition into turbulence were the main features that were captured from the generated flowfield. In the present study, three numerical methods namely, URANS,

*Corresponding author: Mohamed Mohamed
†Email: mohamed.mohamed@southwales.ac.uk

DES and DDES, are developed and applied to evaluate their ability in predicting the large separated flow and it's control over the wall-mounted hump using steady suction and Synthetic Jet Actuator (SJA). The resulting separated flow filed from the hump can be described as a large separation, which it stands between the mild and massive flow separation. The objectives of the present study are to develop and assess the DDES approach in predicting this large separated flow in comparison with URANS and DES methods. Furthermore, to use the dynamic grid techniques in simulating the movement of SJA membrane instead of using the traditional method of applying the oscillating boundary conditions at the jet exit. The numerical results showed that the DDES model was not able to predict the flow physics or separation line in contrast with URANS and DES models. In terms of applying the synthetic jet control, very interesting results were obtained from using the dynamic grid techniques in simulating the cavity flow. These results provided remarkable explanation of the separated flow control mechanism using synthetic jet. An impressive information about the flow physics inside the cavity was declared.

II. NUMERICAL METHODS

A cell-centre finite-volume flow solver with a Spalart-Allmaras (S-A) one equation turbulence model is developed and used in the present study. Parallel computations using MPI environment and domain decomposition technique are applied to improve the performance of numerical simulations. URANS, DES and DDES methods are implemented in this solver, which the turbulent flows are simulated by Navier–Stokes equations in an Arbitrary Lagrangian Eulerian (ALE) framework [24, 25]. The main formulation in the present approaches can be explained briefly as follows:

$$\partial_t \int_{\Omega} \vec{U} dV + \int_{s} \vec{U} F.\hat{n} dS = 0 \tag{1}$$

where $\overrightarrow{U}$ is the state vector and $\overrightarrow{F}$ is flux vector, and both are represented by the following equations:

$$\vec{U} = \begin{pmatrix} \rho \\ \rho\vec{u} \\ E \end{pmatrix} \quad \text{and} \quad \vec{F} = F^c + F^v \tag{2}$$

where

$$F^c = \begin{pmatrix} \rho\vec{u} \\ \rho\vec{u} \bigotimes \vec{u} + P[I] \\ (E+P)\vec{u} \end{pmatrix} \quad \text{and} \quad F^v = \begin{pmatrix} 0 \\ [\tau] \\ ([\tau] \bullet \vec{u}) + \vec{q} \end{pmatrix} \tag{3}$$

In equation (3), ρ is fluid density, $\vec{u}$ is flow velocity, *E* is total energy, *P* is pressure, [I] is the identity tensor and $[\tau]$ is the stress tensor, which is given as:

$$\left[\tau\right] = \left(\mu_L + \mu_{tur}\right)\left[\nabla\vec{u} + \nabla^T\vec{u} - \tfrac{2}{3}(\nabla.\vec{u})[I]\right] \tag{4}$$

In equation (4), the turbulent viscosity μ_T is calculated from the S-A turbulence model [26, 27], which is given as:

$$\frac{D\tilde{\nu}}{D_t} = \underbrace{c_{b_1}\tilde{S}\tilde{\nu}}_{\text{Production Term}} \underbrace{- c_{w_1} f_w P \left(\frac{\tilde{\nu}}{d}\right)^2}_{\text{Destruction Term}} + \underbrace{\frac{1}{\sigma}[\nabla.((\nu+\tilde{\nu}))\nabla\tilde{\nu}) + c_{b2}(\nabla\tilde{\nu})^2]}_{\text{Diffusion Term}} \tag{5}$$

where $\frac{D}{D_t} = \frac{\partial}{\partial_t} + \tilde{\mu}_i \frac{\partial}{\partial x_t}$ is the material derivative and $\tilde{\nu}$ is the modified kinematic eddy viscosity and is defined as, $\tilde{\nu} = \frac{\nu_T}{f_{\nu 1}}$ where, ν_T is the kinematic turbulent viscosity $(\nu_T = \frac{\mu_T}{\rho})$.

The rest of letters in equation (5) are functions coefficients for turbulence closure problem. The model coefficients are given as follows:

c_{b1} = 0.1355, C_{b2}=0.622, $C_{\nu 1}$=7.1, $\sigma = \frac{2}{3}$, κ=0.41,
$c_{w1} = \frac{c_{b2}}{k^2} + \frac{1+c_{b2}}{\sigma}$, $c_{w2} = 0.3$,
$c_{w3} = 2$

The closure functions are defined as:

$\chi = \frac{\tilde{\nu}}{\nu}, f_{v1} = \frac{\chi^3}{\chi^3 + C_{v1}^3}, f_{v2} = \frac{\chi}{1+\chi f_{v1}}, \tilde{S} = S + \frac{\tilde{\nu}}{k^2 d^2} f_{v2}$,
$r = \frac{\tilde{\nu}}{\tilde{S} k^2 d^2}$

$g = r + c_{w2}(r^6 - r), f_w = g\left[\frac{1+c_{w3}^6}{g^6 + c_{w3}^6}\right]^{\frac{1}{6}}$

where *d* is the height of the first grid cell off the wall and *S* is the vorticity, which can be given in terms of the mean-rotation-rate tensor (Ω_{ij}),

$$S = |\Omega| = \sqrt{2\Omega_{ij}\Omega_{ij}}, \text{Where } \Omega_{ij} = \frac{1}{2}\left(\frac{\partial\tilde{u}_i}{\partial x_j} - \frac{\partial\tilde{u}_i}{\partial x_j}\right) \tag{6}$$

In both DES and DDES models, S-A turbulence model is worked as Reynolds Averaged model in the boundary layer region (attached flow) and as Sub-grid Scale model (SGS) in the detached flow region [28]. DES method depends on a new length scale (*d*), in which refers to the wall distance for RANS model and a modified length scale $(\tilde{d})$

ISSN: 2414-4592
DOI: 10.20474/jater-3.5.4

that will replace it and can be defined as:

$$\hat{d} = min(d, C_{DES}\Delta) \tag{7}$$

The symbol C_{DES} is the more effective constant in DES formulation and is taken here as equal to 0.65 [29]. Δ represents the largest dimension of local grid cell, Δ = max $\Delta x, \Delta y, \Delta y$). Accordingly, when $d < C_{DES}, \Delta\tilde{d} = d$, it gets along with RANS region and the model works as the original S-A model. On the other hand, when $d > C_{DES}$, it correlates with the LES region and the model hence acts like the Smagroinsky's SGS model. The DDES model is formulated by conducting a modification to the length scale (d) to delay the early switching from RANS to LES before treating the boundary layer region in RANS mode regardless of grid density [30]. In S-A model, the ration between the length scale and the wall distance (r_d) is slightly adjusted to transfer the information of molecular and eddy viscosity as follows:

$$r_d = \frac{\nu_t + \nu}{\sqrt{U_{i,j}U_{i,j}}\kappa^2 d^2} \tag{8}$$

Where, ν_t is kinematic turbulent viscosity, ν is dynamic viscosity, is velocity gradient tensor, κ is Von Kármán constant and is length scale. This parameter equals to 1.0 in the logarithmic layer and approaches to 0.0 steadily towards the boundary layer edge. The parameter (r_d) is used in the delay function of DDES (f_d) as follows:

$$f_d \equiv 1 - \tanh([8r_d]^3) \tag{9}$$

which it is formulated to be 1.0 in the LES area where $r_d \leq 1$, and 0.0 elsewhere. Consequently, the DES length scale $(\tilde{d})$ is re-defined for DDES model to be as follow:

$$\tilde{d} = d - f_d \max(0, d - C_{DES}\Delta) \tag{10}$$

Thus, by setting $f_d = 0.0$ in the boundary layer region; hence $\tilde{d} = d$, and the DES model always exhibits RANS behaviour and this prevents Modelled Stress Depletion (MSD) from occurring. However, setting $f_d = 1.0$ away from the near wall region, gives $\tilde{d} = C_{DES}\Delta$. Thus, the DDES model will be generated by multiplying the value that can force the A-S model to work like RANS or DES by delaying function f_d.

III. MODEL AND FLOW CONFIGURATIONS

The hump model used in the present study is constructed to be exactly similar to the one that has been used in the experiments [21] The flow configurations of both uncontrolled (baseline) and controlled (steady suction & synthetic jet) cases are performed at experimental Reynolds number of $Re_c = 9.36 \times 10^5$ that is calculated in terms of free stream velocity, $U_\infty = 34.6m/s$ and model chord length, c = 0.42 m [18, 19, 31]. The two active flow control are applied by means of two-dimensional slots located at $x/c \approx 0.65$ along the model spanwise with an opening of 0.00187c, directly upstream on the concave surface. The steady suction control performed at mass flow rate of [19] However, $\dot{m} = 0.01518kg/s$ the synthetic jet control used an actuator with membrane frequency of $f = 183.5Hz$, that gives a peak velocity of $U_p = 26.6m/s$ out the slot [31].

A. Computational Setup

All the simulation results documented here are based on a three-dimensional structured grid has total number of Nx.Ny.Nz = 539.140.28=2,112,880 with extra 134400 cells in case of cavity consideration. 24 grid points are generated along the plenum slot, which provides the flow control of hump's separated flow. The actuator cavity is not included in the solution domain of both uncontrolled and steady suction controlled cases. However, the plenum is included in the synthetic jet control case and an oscillatory membrane is placed at the bottom of the plenum. The solution domain extends to x/c=-6.39 upstream from the hump leading edge and to x/c=4 downstream from the hump leading edge. The location of x/c=-6.39 is chosen to ensure that the boundary layer develops naturally to become fully turbulent and reaches the same thickness as the experiments (δ/h=0.57) at location of x/c=-2.14 upstream model leading edge [19, 32, 33]. The upper wall boundary of the domain is placed at y/c=0.909. Figure 1, shows the hump model layout and domain's dimensions used in the present synthetic jet control.

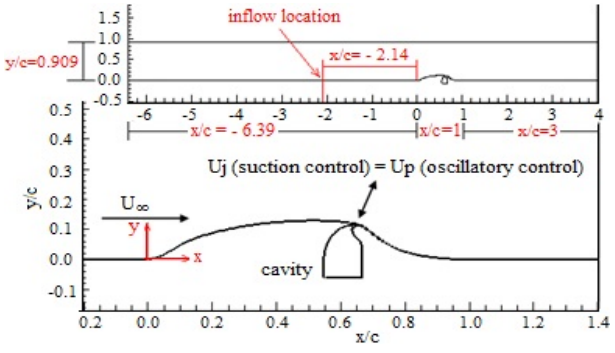

Fig. 1 . Hump model and computational domain outline

ISSN: 2414-4592
DOI: 10.20474/jater-3.5.4

The three-dimensional solution domain is extended by 20% chord length (*Lz* = 0.2c) in the spanwise direction with total dimensions of *Lx*Ly*Lz*=10.39c*0.909c*0.2c, as shown in Figure 2. A uniform resolution of Δz = 0.007 is applied along the spanwise direction, which gives 28 mesh points in *z*-direction. The non-dimensional time step used in the present simulations was $\Delta t = \Delta t^* U_\infty / c$ =0.00021, where Δt^* is the physical time step applied to the solver in seconds. The normal distance between the model wall and the first boundary layer is set at *d* = 2.38*10-5c, which results in $y+ < 1$. ut pairs taken together as a union set.

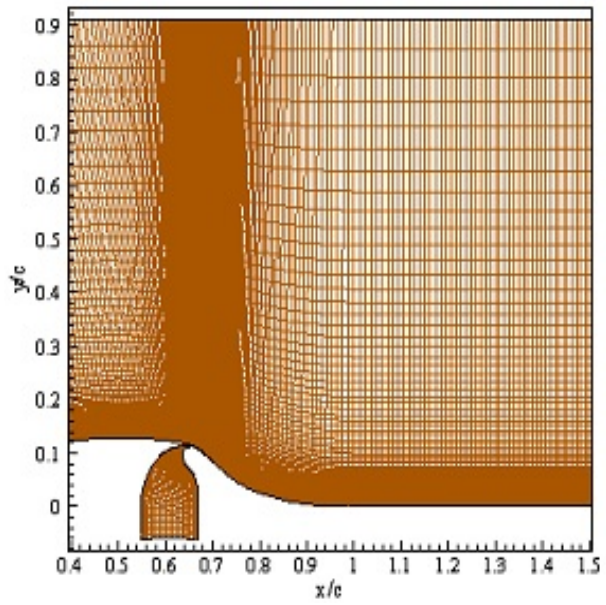

Fig. 2 . Sketch of the 3-D computational domain of flow over a hump

IV. BOUNDARY CONDITIONS

No slip adiabatic boundary conditions were applied at the floor, the hump model and the walls inside the cavity. The far field Riemann-type boundary condition is applied at the front of the solution domain at x/c = -6.39. At the end of solution domain downstream the hump model, the pressure outlet boundary condition is set at x/c = 4, in which the atmospheric pressure was set for the pressure and the other flow quantities were obtained by extrapolation from the interior domain. The wall at the top of the wind tunnel is treated like organised an inviscid wall boundary condition. Finally, the longitudinal sidewalls are treated as symmetry boundary conditions. Figure 3, shows comparison of numerical and measured average velocity profile at distance of x/c = -2.14 from the hump leading edge.

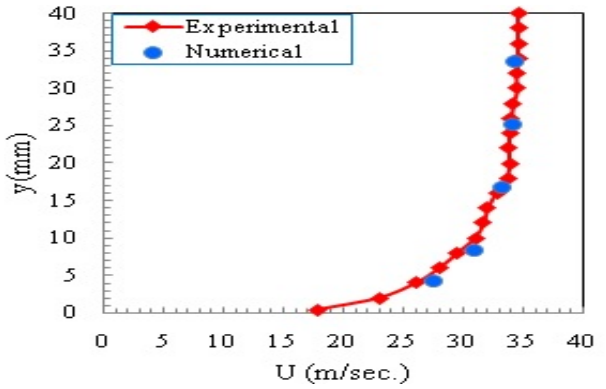

Fig. 3 Comparison of predicted and experimental [27] inflow profile of flow over a hump at x/c = -2.14

ISSN: 2414-4592
DOI: 10.20474/jater-3.5.4

V. RESULTS OF UNCONTROLLED HUMP

A. Separation and Reattachment Locations

The 2D PIV, hot wire and oil film interferometry data have shown that the flow over hump is separated at x/c ≈0.665 and the reattachment line was approximately at x/c ≈1.1. Figures 4 (a), (b), (c) and (d), show comparison of the mean flowfield streamlines as calculated from the experiment and predicted from the present simulations results using URANS, DES and DDES approaches respectively.

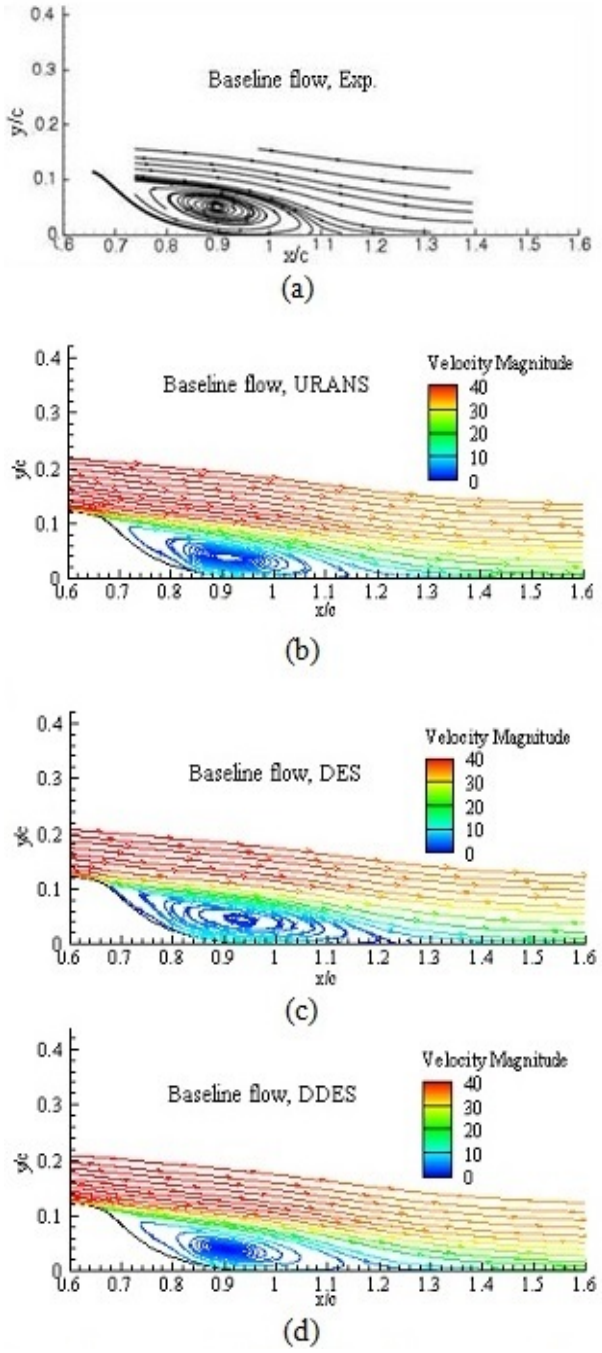

Fig. 4 . Comparison of measured and predicted mean streamlines of uncontrolled hump (a)- Exp.[19], (b)- URANS, (c)- DES and (d)- DDES

ISSN: 2414-4592
DOI: 10.20474/jater-3.5.4

As can be seen in Figure 4, the mean streamlines that predicted by URANS, DES and DDES methods agree fairly well with the measurements. Table 1 shows comparison of predicted and measured separation and reattachment points of the separated flow over the baseline hump. The tabulated results showed that the present numerical methods agree realistically with both measurements and previous numerical simulations. However, the predicted reattachment locations by present models are slightly higher than the experimental measurements.

TABLE 1
COMPARISON OF PREDICTED AND MEASURED SEPARATION AND REATTACHMENT LOCATIONS OVER A STEADY SUCTION CONTROLLED HUMP

Approach	Separation Point	Reattachment Point	
	2D PIV Centreline	Oil Film (Off Centreline)	2D PIV Centreline
Exp. [19]	x/c= 0.665±0.005	x/c=1.11±0.003	x/c=1.10±0.005
	Previous Numerical Simulations		
LES [34]	x/c≈ 0.65	1.090	
LESC [35]	x/c≈ 0.667	1.114	
DES [36]	x/c≈ 0.65	1.130	
URANS [37]	x/c≈ 0.65	1.250	
ILES [38]	x/c≈ 0.65	1.139	
LES [39]	x/c= 0.658	1.079	
	Present Simulations		
URANS	x/c≈ 0.662±0.0002	≈ 1.205	
DES	x/c≈ 0.664±0.0002	≈ 1.194	
DDES	x/c≈ 0.661±0.0002	≈ 1.183	

B. Flow Field Features

Figures 5 (a), (b), (c) and (d), show comparison between the measured and predicted mean streamwise U-velocity component contours of the uncontrolled hump, respectively. As can be seen, the present simulation results are consistent with the measurements in the region starts from somewhat upstream the separation point to the reattachment line, however, the present numerical methods predicted a slightly smaller circulation region compared to the measurements.

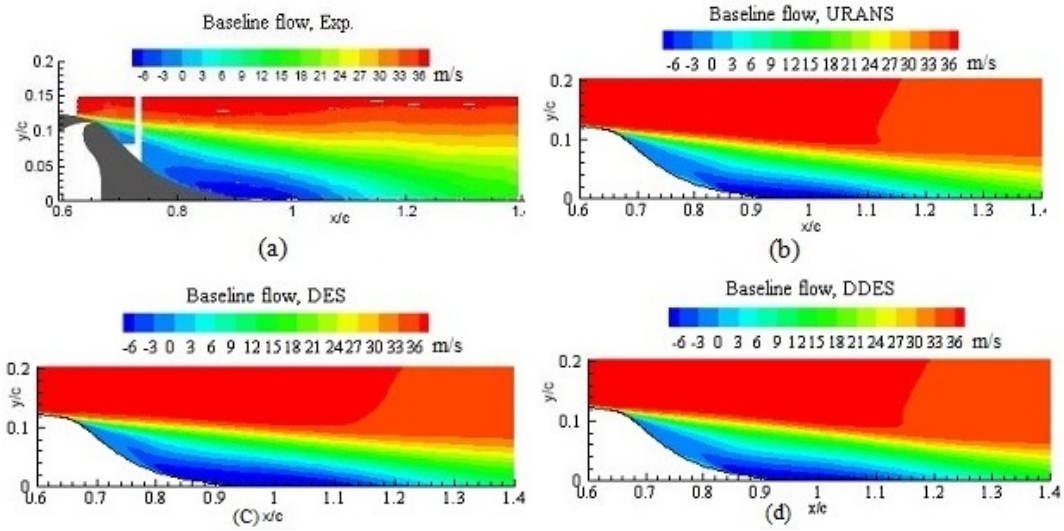

Fig. 5 . Comparison of measured and predicted mean streamwise U-component contours of uncontrolled hump (a) -Exp. [19], (b) -URANS, (c) -DES and (d) -DDES

ISSN: 2414-4592
DOI: 10.20474/jater-3.5.4

C. Q_Criteria

Figures 6 (a), (b) and (c), show the predicted iso-surface of instantaneous Q_criteria field of the flow over uncontrolled hump using present numerical methods. As can be seen, URANS and DDES methods provided steady solutions and they do not show the flow unsteadiness in the separated flow region after the hump aft part of the hump model. On contrary, the DES method captured successfully the turbulent flowfield with varies turbulent scales as shown in Figure 6 (b).

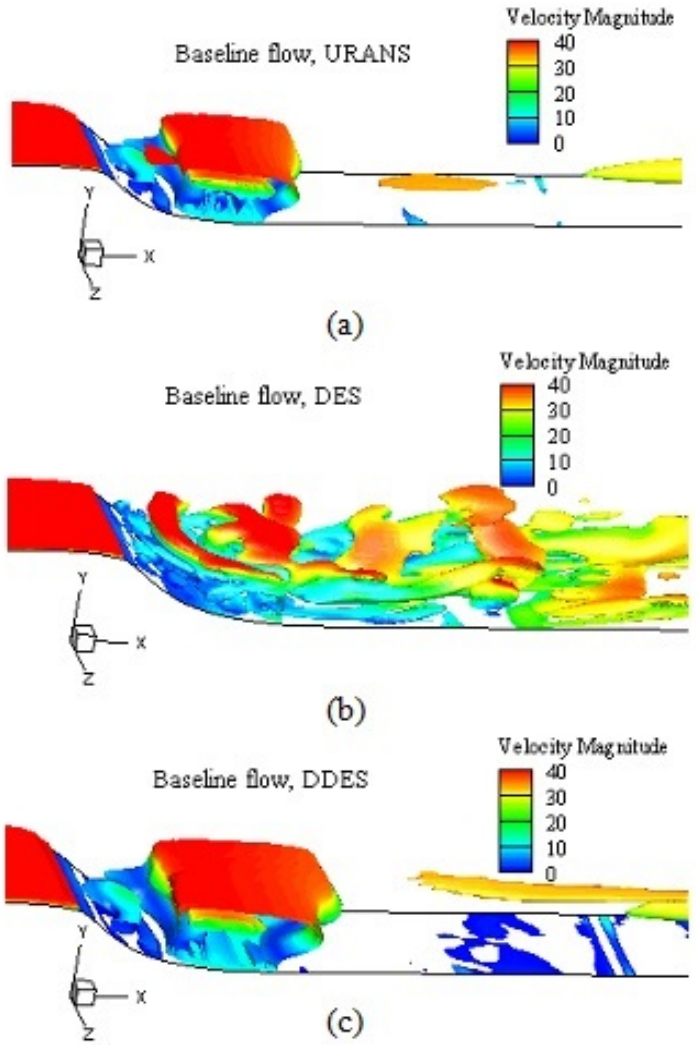

Fig. 6 Iso-surface of the predicted instantaneous Q_criteria field of uncontrolled hump, (a)-URANS, (b)-DES and (c)-DDES

D. Mean surface pressure distributions (Cp)

Figures 7 (a), (b) and (c), show compassion of the measured predicted and mean surface pressure distributions over uncontrolled hump. The Figures showed that the flow over the hump stays attached to the hump surface with reduction in pressure until reaches to the beginning of the ramp region (strong convex surface) at approximately $x/c \approx 0.6$, then the pressure increases greatly due to the boundary layer separation at nearly $x/c \approx 0.665$. After separation occurs, the flow stays separated in the aft region before it reattaches again downstream the model trailing edge at about $x/c \approx 1.1$. As demonstrated in the Figures below, the predicted surface pressure coefficients are in decent agreement with the measurements. However, the predicted pressure coefficients quite bigger than measured values downstream the reattachment line, which agree with previous numerical simulations [33, 34, 40].

ISSN: 2414-4592
DOI: 10.20474/jater-3.5.4

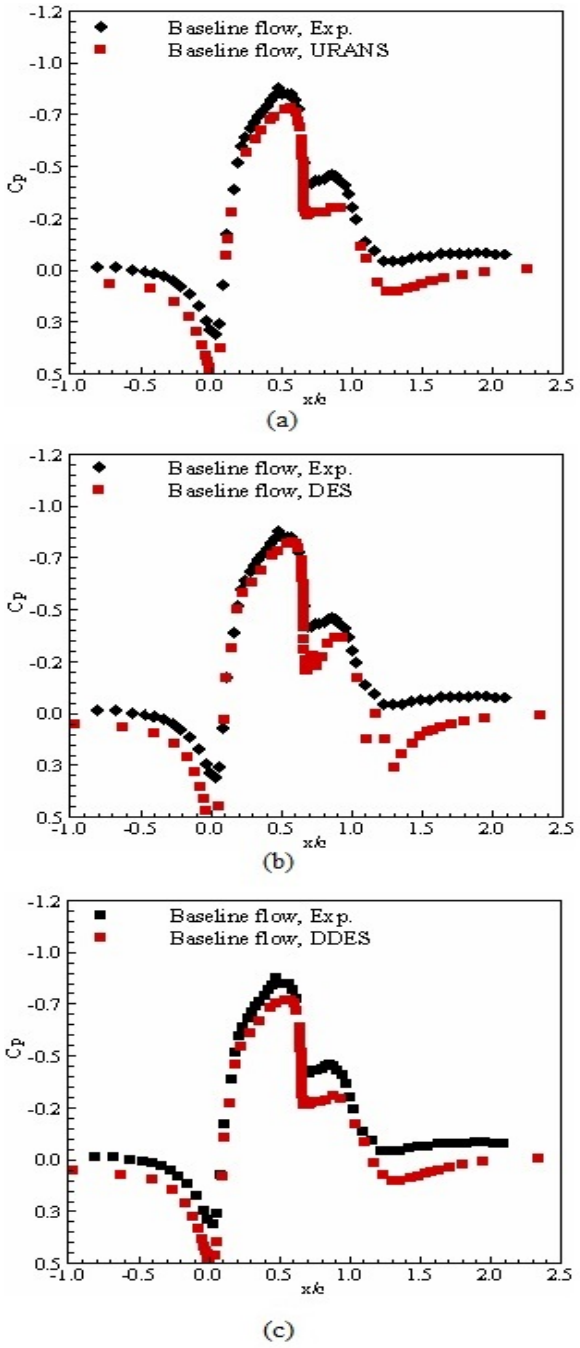

Fig. 7 Comparison of measured and predicted mean pressure distributions over uncontrolled hump
(a)-URANS, (b)-DES, (c)-DDES

VI. RESULTS OF STEADY SUCTION CONTROL

A. Separation and Reattachment Location

The experimental measurements using 2D PIV, hotwire and oil film techniques showed that the flow over hump is separated at x/c ≈ 0.680, and the reattachment occurred at x/c ≈ 0.92 -0.94, when the steady suction control was applied. Figures 8 (a), (b), (c), and (d) show comparison of measured and predicted mean flowfield over steady suction controlled hump, respectively. The comparison indicates that the results obtained from the three numerical models agree well with the measurements.

ISSN: 2414-4592
DOI: 10.20474/jater-3.5.4

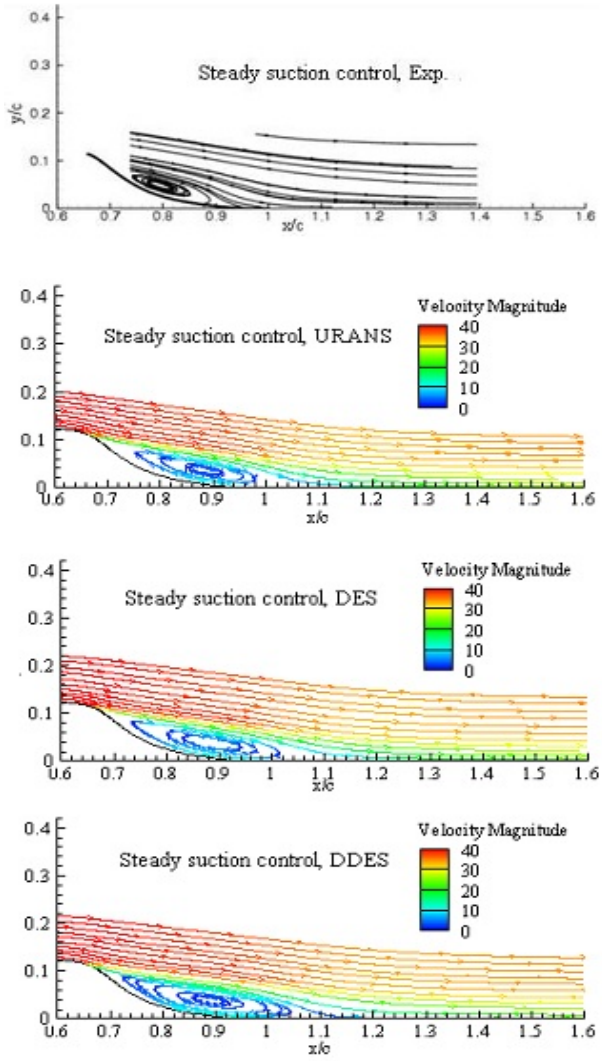

Fig. 8 Comparison of experimental and predicted mean streamlines of steady suction controlled hump; (a)-Exp. [19] (b)-URANS, (c)-DES, (b)-DDES

TABLE 2
COMPARISON OF PREDICTED AND MEASURED SEPARATION AND REATTACHMENT LOCATIONS OVER A STEADY SUCTION CONTROLLED HUMP

Approach	Separation Point	Reattachment Point	
	2D PIV Centreline	Oil Film (off Centreline)	2D PIV Centreline
Exp. [19]	x/c=0.680±0.005	x/c=94±0.005	x/c=0.92±0.005
	Previous Numerical Results		
LES [34]	x/c≈0.65	0.95	
LESC[35]	x/c≈0.65	0.947	
URANS [37]	x/c≈0.65	1.08	
ILES[38]	x/c≈0.65	0.984	
	Present Results		
URANS	x/c≈0.6677	≈0.985	
DES	x/c≈0.663	≈1.041	
DDES	x/c≈0.667	≈1.076	

ISSN: 2414-4592
DOI: 10.20474/jater-3.5.4

Furthermore, Table 2 shows comparison of the predicted and measured locations of separation and reattachment lines of the steady suction controlled flow over hump model. Indubitably, the present numerical methods predicted the separated flow point in reasonable agreement with the experimental measurements and quite better than previous simulations. However, they over-predicted the reattachment line and this agrees with the previous numerical simulations as documented in Table 2. On the other hand, URANS approach gives the best agreement (x/c ≈ 0.985) with the measurements compared to the DES (x/c ≈ 1.041) and DDES (x/c ≈ 1.076) approaches.

B. Flow Field Features

The turbulent flowfield characteristics of the steady suction controlled flow over a hump model as predicted by the present simulation method in comparison with experimental data available are presented in this part in terms of mean stream wise U-velocity component contours and the instantaneous Q_criteria field.

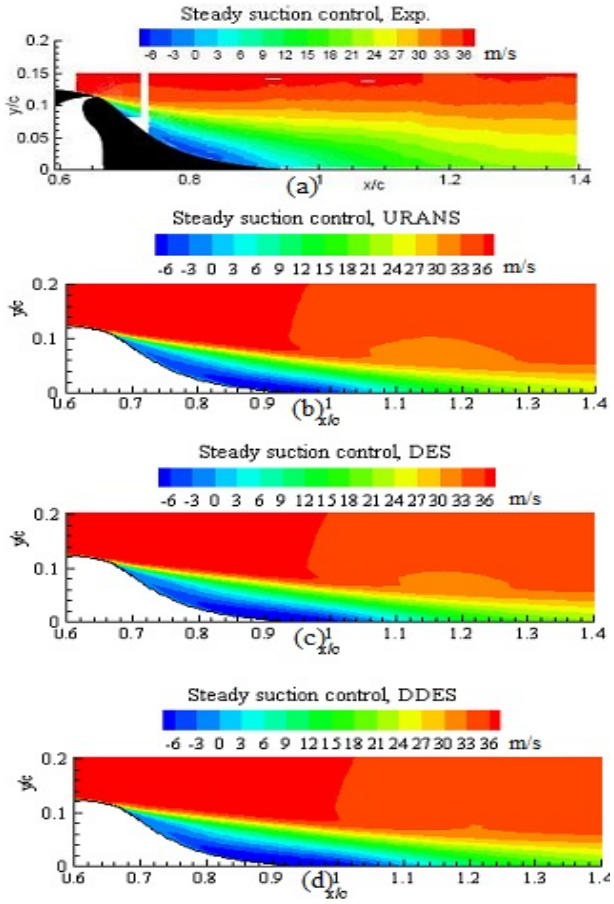

Fig. 9 Comparison of experimental and predicted mean streamwise U-component (m/s) contours of steady suction controlled hump (a)-Exp. [19] (b)-URANS, (c)-DES, (b)-DDES

Figures 9 (a), (b), (c), and (d) show comparison of the mean stream wise U-velocity component (m/s) contours of controlled flow over a hump model as calculated from the experiment and present simulation with URANS, DES and DDES approaches respectively. As can be seen, URANS, DES and DDES approaches predicted a quite big separation zone in comparison with the experimental data, hence over-predicted the reattachment line, as discussed in previous section.

ISSN: 2414-4592
DOI: 10.20474/jater-3.5.4

C. Q_Criteria

Figures 10 (a), (b) and (c), show comparison of the predicted iso-surface of Q_criteria field of the steady suction controlled hump with experimental data. The results obtained by applying steady suction control are quite similar with the uncontrolled hump results in section 6. 3. The Figures show that, both the URANS and DDES methods provide steady solutions and they cannot predict the flow unsteadiness in the controlled flow after the hump aft part of the hump model. On the other hand, the DES approach captured successfully the flow unsteadiness in the controlled flow as illustrated in Figure 10 (c). Moreover, the steady suction control technique alleviated the intensity of the fluctuation in the controlled flow as seen in Figure 10 (c) as compared to the uncontrolled hump in Figure 6 (c).

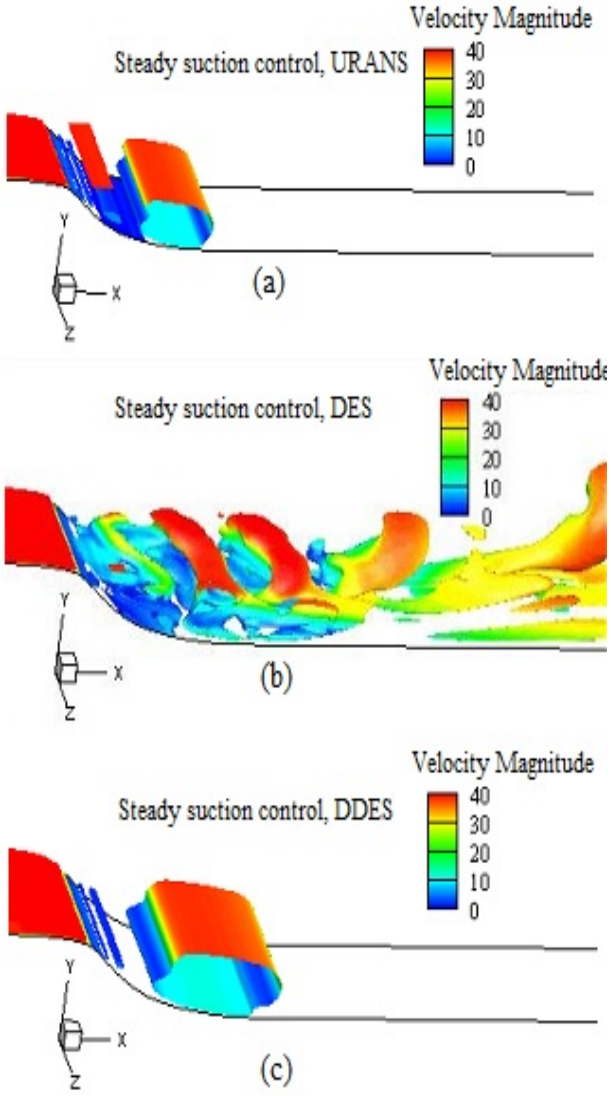

Fig. 10 . Iso-surface of the predicted instantaneous Q_criteria field of steady suction controlled hump using present numerical methods, (a)-URANS, (b)-DES, (c)-DDES

D. Mean surface Pressure Distributions (Cp)

Figures 11 (a), (b) and (c) show comparison between the predicted and measured values of mean surface pressure coefficient of hump separated flow that controlled by steady suction control technique. The measured surface pressure coefficient indicates clearly that the flow over the hump remains attached to the surface until it reaches the

ISSN: 2414-4592
DOI: 10.20474/jater-3.5.4

beginning of the ramp region at x/c≈0.6, then the pressure increases significantly due to the boundary layer separation at approximately x/c≈0.68. The flow stays separated in the aft part of the model before it reattaches again downstream of the model trailing edge at x/c≈0.94. While, the predicted values of surface pressure coefficient are in decent agreement with the measured values, the predicted pressure coefficient lines are shifted below the experimental in the region close to the reattachment point of each numerical model. This behaviour is quite similar to the uncontrolled case and agrees with previous numerical simulations [33, 34, 41].

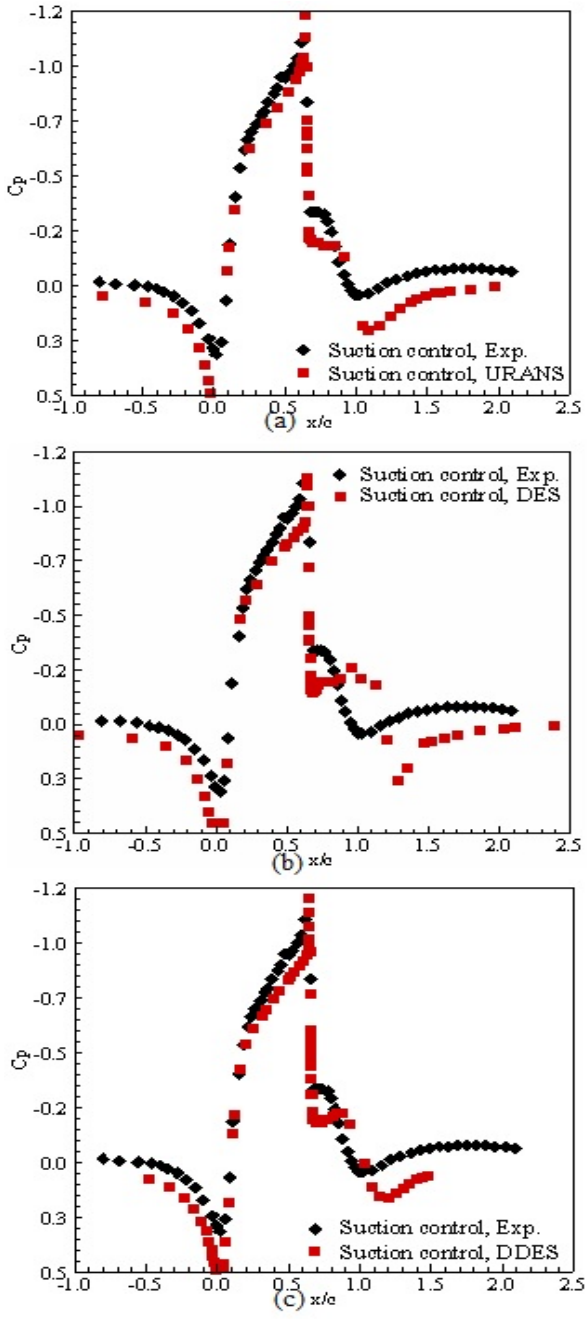

Fig. 11 . Comparison of predicted and experimental mean pressure distributions over steady suction controlled hump(a)-URANS, (b)-DES, (c)-DDES

ISSN: 2414-4592
DOI: 10.20474/jater-3.5.4

VII. RESULTS OF SYNTHETIC JET CONTROL

A. Control Mechanism of SJA

Figures 12 (a), (b), (c) and (d), show schematic diagrams of the oscillatory suction/blowing actuating system that attached to hump model and the operating strokes during the SJA flow control, respectively.

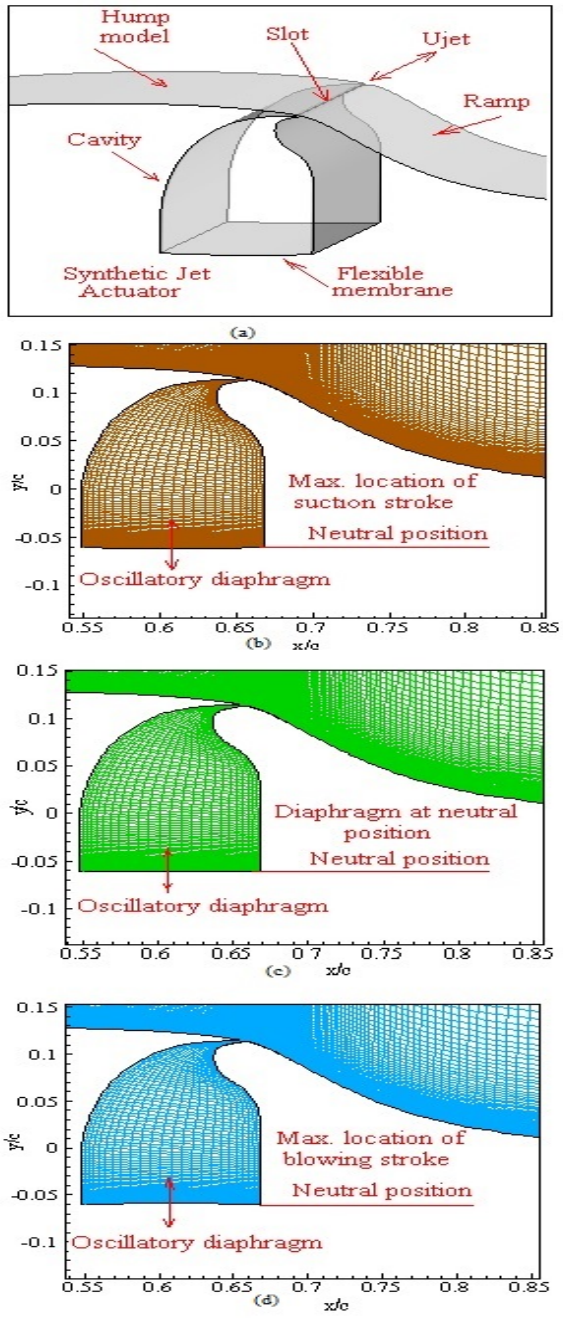

Fig. 12 . Outlines of the SJA actuator and its operating cycle, (a)-hump model equipped with SJA, (b)-suction stroke, (c)-neutral position (d)-blowing stroke

B. Separation and Reattachment Location

The experimental measurements of the hump flowfield controlled by SJA indicated that the flow separates at x/c≈0.676 and reattaches again to the surface at x/c≈0.98. Figures 13 (a) and (b) show comparison of predicted and measured mean streamlines flowfield of synthetic jet controlled hump. As can be seen, the predicted mean streamlines by DES method with applying dynamic grid technique agrees reasonably well with the experimental measurements, however the size of the separation zone is quite small in case of the DES simulations as indicated in Figure 13 (b).

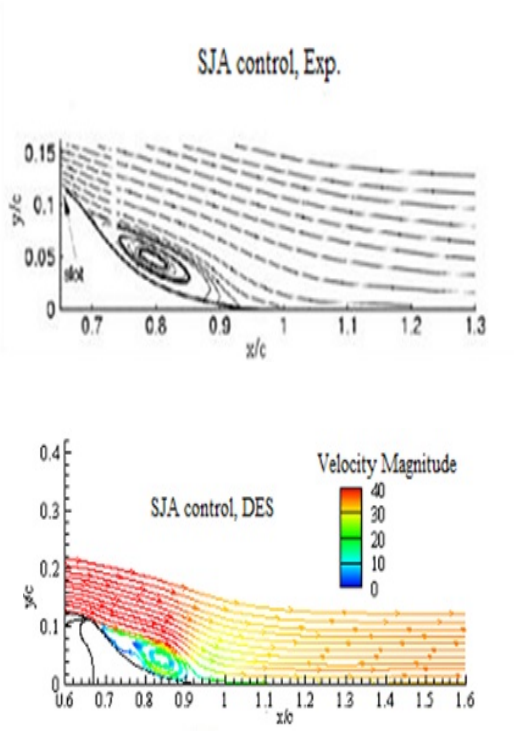

Fig. 13 . Comparison of experimental and predicted mean flowfield
streamlines of SJA controlled hump, (a)-Exp.[31], (b)-DES.

Table 3 shows comparison of measured and predicted locations of separation and reattachment points for the controlled hump flow using SJA. As demonstrated in the table below, the location of separation point that predicted by present DES model agrees in a sensible way with measurements and previous LES model [39], however the reattachment point is quite smaller. On the other hand, the simulation results from present DES approach are quite good compared to the previous numerical simulations.

ISSN: 2414-4592
DOI: 10.20474/jater-3.5.4

TABLE 3
COMPARISON OF MEASURED AND PREDICTED SEPARATION AND REATTACHMENT LOCATIONS OVER A SJ CONTROLLED HUMP

Approach	Separation Point	Reattachment Point	
	2D PIV Centreline	Oil Film (Off Centreline)	2D PIV Centreline
Exp. [31]	x/c=0.676	x/c=0.98	
	Previous Numerical Results		
LES [34]	x/c≈0.65	1.01	
LESC[35]	x/c≈0.65	1.020	
ILES[38]	x/c≈0.65	1.097	
LES[39]	x/c≈0.674	0.979	
	Present Results		
DES	x/c ≈0.6695	≈0.963	

C. Flow Field Features

Figures 14 (a) and (b), show comparison of the mean streamwise U-velocity component (m/s) contours of the synthetic jet controlled flow over a hump model as predicted by the present DES code and the experiments, respectively. As can be seen, the present DES approach failed to predict accurately the reattachment line downstream the ramp region and there is a discrepancy between the predicted mean streamwise U-velocity pattern and the measured one in the separated flow region.

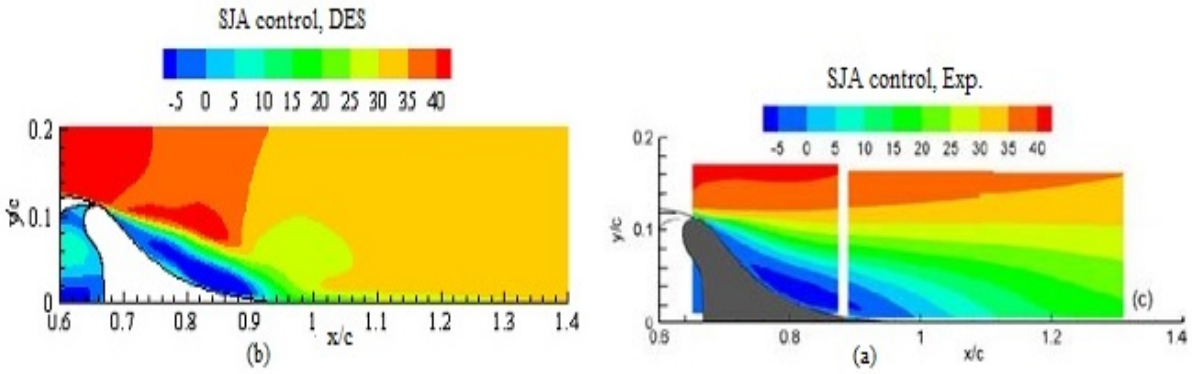

Fig. 14 . Comparison of experimental and predicted mean streamwise U-component (m/s) contours of SJA controlled hump (a)-Exp. [31], (b)-DES

Very interesting results are obtained from the present simulations in the interface region between the plenum flow and the near wall vicinity flow, where the separated boundary layer existed. As can be seen from Figure 15, there are two counter rotating vortices existed inside the plenum during the control cycle of the SJA, which they move up and down during suction and blowing strokes and finally energize the detached boundary layer in the separated flow region. The results showed that the control efficiency of the SJA depend on the flow interaction between the vortical flow inside the plenum and the flow inside the separated boundary layer.

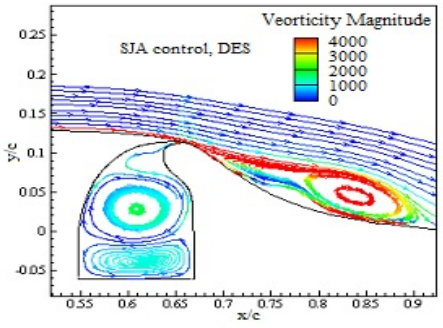

Fig. 15 . Flow interaction between actuator cavity flow and separated boundary layer of a SJ controlled hump as predicted by DES model.

ISSN: 2414-4592
DOI: 10.20474/jater-3.5.4

D. Mean Surface Pressure Distributions (Cp)

Figure 16 shows comparison of experimental and simulated mean surface pressure coefficient over the SJ controlled hump. As can be seen, the flow over SJ controlled hump remains attached to the hump surface long time compared to the uncontrolled and the steady suction controlled cases. The flow does not separate until it reaches the beginning of the ramp region and passes the slot. Then, the boundary layer separates at approximately x/c≈0.67 and the pressure coefficient increases sharply and due to the strong adverse pressure phenomenon. Moreover, the flow stays separated in the aft part of the model before it reattaches quickly downstream the model trailing edge at x/c≈0.963 as illustrated indicated in Table 3. The predicted pressure coefficient of the SJ controlled flow close to the measured values in the region directly before the separation occurs. However, there are discrepancies in the predicted pressure coefficient values in the separation region.

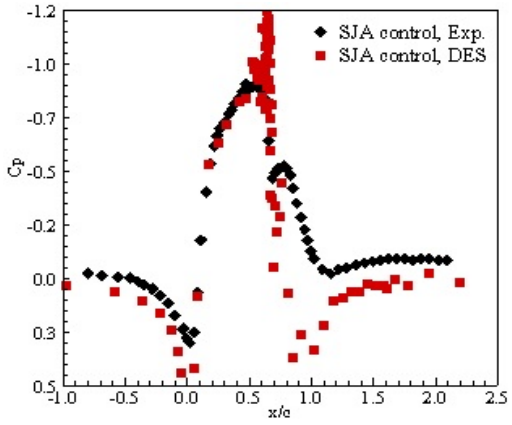

Fig. 16 . Comparison of experimental [31] and predicted mean pressure distributions over a SJA controlled hump

E. Phase-Averaged Spanwise Vorticity Field

Figures 17 (a-1), show twelve contour plots of phase-averaged spanwise vorticity (ωz) field of the experimental measurements and DES simulation results for comparison. As can be seen from the plots, the blowing part of the cycle starts at phase φ = 30°,in which the free shear layers downstream the slot are moved downstream away from the hump surface. This feature of the flow distinguishes the suction stroke that has just proceeded the blowing cycle. As the membrane moves up, the blowing cycle reaches the peak at phase φ = 90°, in which the shear layer just lifted off the wall, will distort and a reverse flow region will generate all over the hump surface. This distorted shear layer distinguishes the vortex rolling up and decreasing the pressure downstream of the slot. As the blowing stroke diminishes at phase φ = 150°, the previous vortices move downstream the ramp region and energize the reverse flow region near the wall. As the control switches from blowing stroke to suction stroke at phase φ = 210°, these vortices start to diminish and move away from the shear layer. At the peak of the suction cycle at phase φ = 270°, the shear layer is dragged close to the wall near the slot and curved shear layer is generated. At the end of suction cycle at phase=330°, the vortex breaks free and moves with the flow downstream of the ramp region. The plots show that, the present DES approach does not predict the spanwise vorticity (ωz) field compared to the experiments and the predicted vortices linked together in a steady manner. This is might be due to small number of the operating cycles that used to calculate the phase-averaged field and bigger time step value.

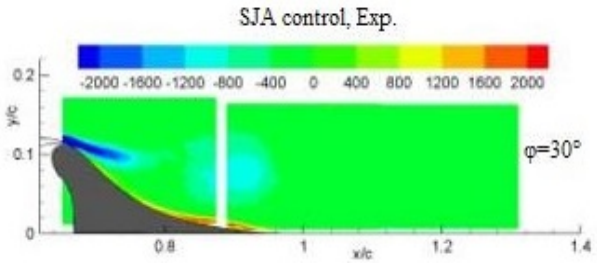

. (a)-φ = 30°, Exp

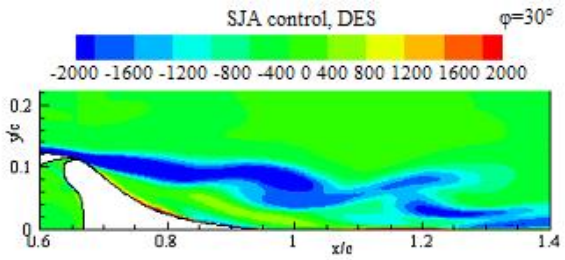

(b)- φ = 30°, DES

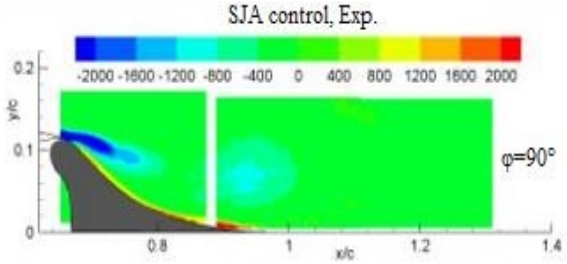

(c)-φ = 90°, Exp.

ISSN: 2414-4592
DOI: 10.20474/jater-3.5.4

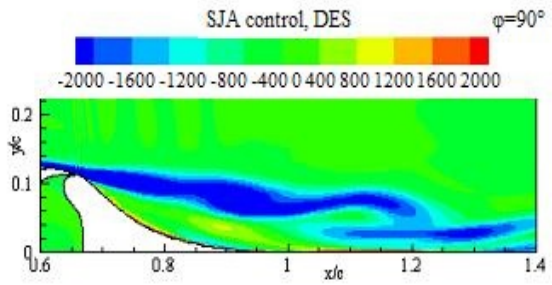

(d)- φ = 90°, DES

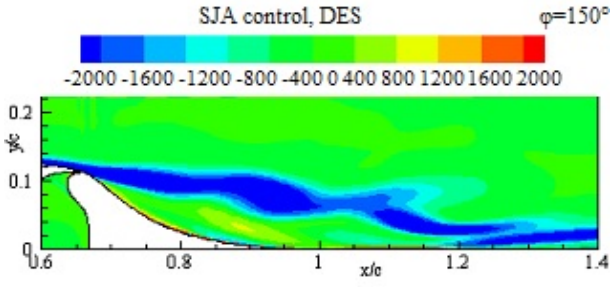

(e)-φ = 150°, Exp.

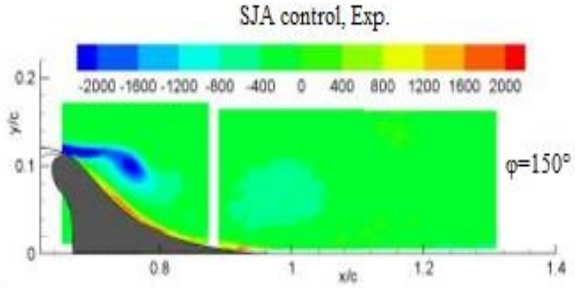

(e)-φ = 150°, DES

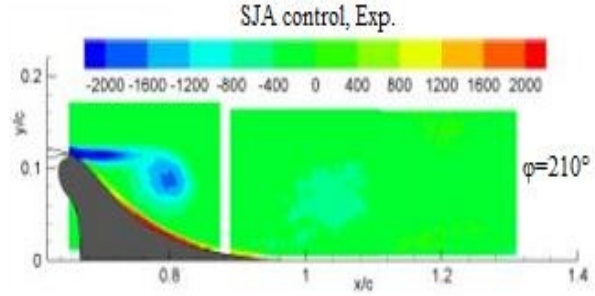

(g)-φ = 210°, Exp.

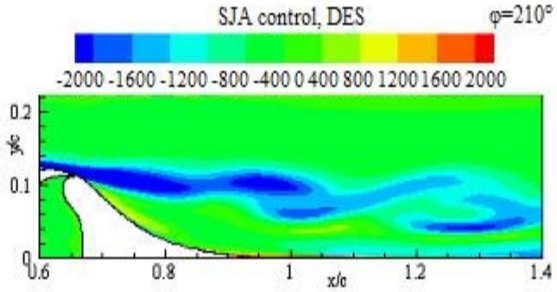

(h)- φ = 210°, DES

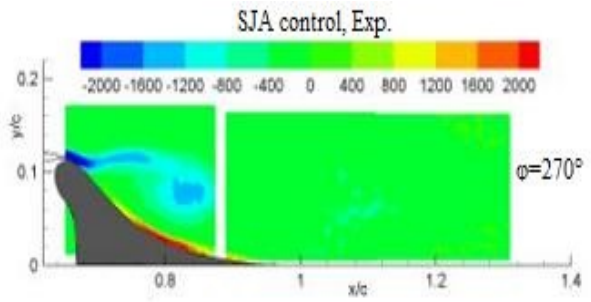

(i)-φ = 270°, Exp.

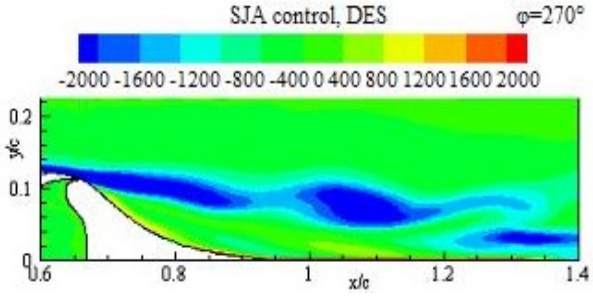

(j)- φ=270°, DES.

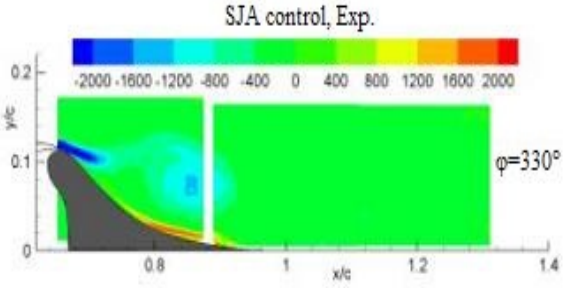

(k)-φ=330°, Exp.

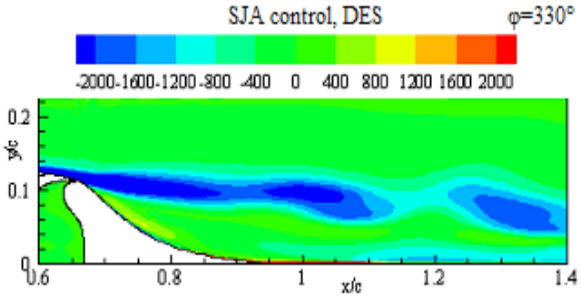

(l)- φ=33°, DES.

Fig. 17 . Comparison of experimental [31] and DES predicted phase-averaged spanwise vorticity (ωz) field at six phases of SJ control cycle.

ISSN: 2414-4592
DOI: 10.20474/jater-3.5.4

VIII. CONCLUSION

Three different codes based on URANS, DES and DDES approaches have been developed and applied to study the large separated flow over a hump model and its control using steady suction and synthetic jets. The simulation results obtained from both baseline and controlled cases showed that both URANS and DES methods provides reasonable results compared to experimental data, however DDES method failed to predict the mean flowfied characteristics or flow unsteadiness of such type of flow separation. This is because the DDES model has been originally proposed to avoid the Modelled-Stress Depletion (MSD) problem in attached boundary layer in DES approach by considering the whole boundary layer in URANS mode. Hence, the DDES results matched closely with URANS one in contrast with the DES results for the mean flow properties. The results of steady suction control using the three numerical approaches showed that the separation bubble is effectively reduced; hence, the static surface pressure over the centre of the hump is uniform compared to the baseline case. Only DES approach captured the unsteady features in the turbulent flowfield with a wide range of turbulent scales. The results of synthetic jet control with dynamic grid technique showed very interesting results for the flow interaction between the actuator cavity and the near wall vicinity, where the large separated boundary layer existed. The results showed that, there are two counter rotating vortices existed inside the cavity during the control operating cycle of the SJA that move up and down during suction and blowing strokes of the control cycle and finally energize the retarded boundary layer in the separated flow region.

REFERENCES

[1] L. P. Melton, J. Hannon, C. S. Yao and J. Harris, "Active flow control at low Reynolds numbers on a NACA 0015 airfoil", *in 26th Applied Aerodynamics Conference*, Honolulu, HI, 2008.

[2] L. P. Melton, C. S. Yao and A. Seifert, "Active control of separation from the flap of a supercritical airfoil," *American Institute of Aeronautics and Astronautics*, vol. 44, no. 1, pp. 34-41, 2006. **DOI:** 10.2514/1.12225

[3] R. Petz and W. Nitsche, "Active separation control on the flap of a two-dimensional generic high-lift configuration," *Journal of Aircraft*, vol. 44, no. 3, pp. 865-874, 2007.
DOI: 10.2514/1.25425

[4] A. Seifert, A. Darabi and I. Wygnanski, "Delay of airfoil stall by periodic excitation" *Journal of Aircraft*, vol. 33, no. 4, pp. 691-698, 1996. **DOI:** 10.2514/3.47003

[5] A. Seifert and L. G. Pack, "Oscillatory control of separation at high Reynolds numbers". *American Institute of Aeronautics and Astronautics (AIAA) Journal*, vol. 37, no. 9, pp. 1062-1071, 1999. **DOI:** 10.2514/3.14289

[6] A. Seifert and L. G. Pack, "Oscillatory excitation of unsteady compressible flows over airfoils at flight Reynolds numbers", *in 37th Aerospace Sciences Meeting and Exhibit*, Hampton, VA: NASA Langley Research Center, 1999. **DOI:**10.2514/6.1999-925

[7] A. Siefert, T. Bachar, D. Koss, M. Shepshelovich and I. Wygnanski, "Oscillatory blowing: A tool to delay boundary-layer separation" *American Institute of Aeronautics and Astronautics Journal*, vol. 31, no. 11, pp. 2052-2060, 1993. **DOI:** 10.2514/3.49121

[8] B. L. Smith and A. Glezer, "The formation and evolution of synthetic jets," *Physics of Fluids*, vol. 10, no. 9. pp. 2281-2297, 1998. **DOI:** 10.1063/1.869828

[9] A. Tuck and J. Soria, "Active flow control over a NACA 0015 airfoil using a ZNMF Jet," *in 15th Australasian Fluid Mechanics Conference*, Sydney, Australia, The University of Sydney, 2004.

[10] A. Tuck and J. Soria, "Separation control on a NACA 0015 airfoil using a 2D micro ZNMF jet," *Aircraft Engineering and Aerospace Technology*, vol. 80, no. 2, pp. 175-180, 2008. **DOI:** 10.1108/00022660810859391

[11] C. Yao, F. Chen, D. Neuhart and J. Harris, "Synthetic jet flow field database for CFD validation," *in 2nd AIAA Flow Control Conference*, Portland, OR, 2004. **DOI:**10.2514/6.2004-2218

[12] K. Zaman and I. Milanovic, "Synthetic jets in crossflow," *AIAA Journal*, vol. 43, no. 5, pp. 929-940, 2003.

[13] J. A. Ekaterinaris, "Prediction of active flow control performance on airfoils and wings", *Aerospace Science and Technology*, vol. 8, no. 5, pp. 401-410, 2004.
DOI: 10.1016/j.ast.2004

[14] L. Huang, P. G. Huang, R. P. Le Beau and T. Hauser, "Numerical study of blowing and suction control mechanism on NACA0012 airfoil", *Journal of Aircraft*, vol. 41, no. 5, pp. 1005-1013, 2004. **DOI:** 10.2514/1.2255

[15] V. Kitsios, R. B. Kotapati, R. Mittal, A. Ooi, J. Soria and D. You, "Numerical simulation of lift enhancement on a NACA 0015 airfoil using ZNMF jets," in *Proceedings of the Center for Turbulence Research Summer Program*, Stanford, CA: Stanford University, 2006.

ISSN: 2414-4592
DOI: 10.20474/jater-3.5.4

[16] C. Warsop, M. Hucker, A. J. Press and P. Dawson, "Pulsed air-jet actuators for flow separation control," *Flow, Turbulence and Combustion*, vol. 78, no. 4, pp. 255-281, 2007. **DOI:** 10.1007/s10494-006-9060-4

[17] J. Yan and Y. Xin, "Oscillatory blowing control numerical simulation of airfoil flutter by high-accuracy method," *Journal of Aircraft*, vol. 41, no. 3, pp. 610-615, 2004. **DOI:** 10.2514/1.653

[18] Langley Research Center Workshop, "*CFD validation of synthetic jets and turbulent separation control*," Willimasburg, VA: March, 29-31, 2004. (http://cfdval2004.larc.nasa.gov)

[19] D. Greenblatt, K. B. Paschal, C. Yao, J. Harris, N. W. Schaeffler and A. E. Washburn, "A separation control CFD validation test case part 1: Baseline & steady suction", *in 2nd AIAA Flow Control Conference, Portland*, OR, 2004. **DOI:** 10.2514/6.2004-2220

[20] N. W. Schaeffler and L. N. Jenkins, "Isolated synthetic jet in crossflow: Experimental protocols for a validation dataset". *American Institute of Aeronautics and Astronautics (AIAA) Journal*, vol. 44, no.12, pp. 2846-2856, 2006. **DOI:** 10.2514/1.13743

[21] A. Seifert and L. G. Pack, "Active flow separation control on wall-mounted hump at high Reynolds numbers," *AIAA Journal*, vol. 40, pp. 7, pp. 1363-1372, 2002. **DOI:** 10.2514/2.1796

[22] J. Lim, L. Yue, Y. Na and S. Kim, "Four cases of production-installation simulation for free-form concrete panels," *Journal of Advances in Technology and Engineering Research*, vol. 2, no. 1, pp. 22-27, 2016. **DOI:** 10.20474/-jater2.1.5

[23] S. M. Phyoe, Y. X. Lee and Z. W. Zhong, "Determining the future demand: Studies for air traffic forecasting," *International Journal of Technology and Engineering Studies,* vol. 2, no. 3, pp. 83-86, 2016. **DOI:** 10.20469/ijtes.2.40004-3

[24] J. S. Baggett, "*On the feasibility of merging LES with RANS for the near-wall region of attached turbulent flows*", Stanford, CA: Center for Turbulence Research, 1998.

[25] S. Dahlström and L. Davidson, "*Hybrid RANS/LES employing interface condition with turbulent structure*," 2003 [Online]. Available: goo.gl/9fokTG

[26] P. R. Spalart and S. R. Allmaras, "One-equation turbulence model for aerodynamic flows," *Recherche Aerospatiale*, vol. 5, no. 5, pp. 5-21, 1994.

[27] P. R. Spalart, W. H. Jou, M. Streletes and S. R. Allmaras, "Comments on the feasibility of les for wings and a hybrid RANS/LES approach," *in 1st AFOSR International Conference on DNS/LES*, Ruston; LA, 1997.

[28] A. Travin, M. Shur, M. Strelets and P. S. Palart, "Detached-eddy simulations past a circular cylinder," *Flow, Turbulence and Combustion*, vol. 63, no. 1, pp. 293-313, 2000. **DOI:** 10.1023/A:1009901401183

[29] M. Shur, P. R. Spalart, M. Strelets and A. Travin, "Detached-Eddy simulation of an airfoil at high angle of attack", *in 4th International Symposium on Engineering Turbulence Modelling and Measurements, Elsevier Science*, UK: Oxford Press, pp. 669-678, 1999. **DOI:** 10.1016/B978-008043328-8/50064-3

[30] P. R. Spalart, S. Deck, M. L. Shur, K. D. Squires, M. K. Strelets and A. Travin, "A new version of detached-eddy simulation, resistant to ambiguous grid densities" *Theoretical and Computational Fluid Dynamics*, vol. 20, no. 3, pp. 181-195, 2006. **DOI:**10.1007/s00162-006-0015-0

[31] D. Greenblatt, K. B. Paschal, C. S. Yao and J. Harris, "A separation control CFD validation test case part 2. Zero efflux oscillatory blowing," *in 43rd AIAA Aerospace Sciences Meeting and Exhibit-Meeting Papers*, Reno, NV, 2005. **DOI:** 10.2514/6.2005-485

[32] S. Noelting, M. Wessels, A. Keating, R. Satti, Y. Li and R. Shock, "Lattice Boltzmann simulations of the flow over a hump with flow control," in *Collection of Technical Papers-AIAA Applied Aerodynamics Conference*, Honolulu, HI, 2008.

[33] C. L. Rumsey, "Reynolds-averaged Navier-stokes analysis of zero efflux flow control over a hump model," *Journal of Aircraft*, vol. 44, no. 2, pp. 444-452, 2007. **DOI:** 10.2514/1.23514

[34] D. You, M. Wang and P. Moin, "Large-eddy simulation of flow over a wall-mounted hump with separation control," *American Institute of Aeronautics and Astronautics Journal*, vol. 44, no. 11, pp. 2571-2577, 2006.

[35] S. Sari, S. Jakirli, A. Djugum and C. Tropea, "Computational analysis of locally forced flow over a wall-mounted hump at high-re number". I*nternational Journal of Heat and Fluid Flow*, vol. 27, no. 4, pp. 707-720, 2004.

[36] V. Krishnan, K. D. Squires and J. R. Forsythe, "Prediction of separated flow characteristics over a hump using RANS and des," *in 2nd AIAA Flow Control Conference, Fluid Dynamics and Co-located Conferences*, Portland, OR, 2004. **DOI:** 10.2514/6.2004-2224

[37] F. Capizzano, P. Catalano, C. Marongiu and P. L. Vitagliano, "U-RANS modelling of turbulent flows con-

trolled by synthetic jets", *in 35th AIAA Fluid Dynamics Conference and Exhibit*, Toronto, Canada, 2005. **DOI:** 10.2514/6.2005-5015

[38] P. E. Morgan, D. P. Rizzetta and M. R.Visbal, "Numerical investigation of separation control for flow over a wall mounted hump," in *American Institute of Aeronautics and Astronautics Conference*, Portland, OR, 2004. **DOI:**10.2514/6.2004-2510

[39] A. Avdis, S. Lardeau and M. Leschziner, "Large eddy simulation of separated flow over a two-dimensional hump with and without control by means of a synthetic slot-jet," *Flow, Turbulence and Combustion*, vol. 83, no. 3, pp. 343-370, 2009. **DOI:** 10.1007/s10494-009-9218

[40] C. L. Rumsey, T. B. Gatski, W. L. Sellers, V. N. Vatsa and S. A. Viken, "CFD validation of synthetic jets and turbulent separation control", in *Langley Research Center Workshop*, Williamsburg, VA, 2004. **DOI:** 10.2514/6.2004-2217

[41] C. L. Rumsey, T. B. Gatski, W. L. Sellers, V. N. Vatsa and S. A. Viken, "Summary of the 2004 computational fluid dynamics validation workshop on synthetic jets" *AIAA Journal*, vol. 44, no. 2, pp. 194-204. 2006. **DOI:** 10.2514/1.12957

— This article does not have any appendix. —

ISSN: 2414-4592
DOI: 10.20474/jater-3.5.4